Introduction to Spectroscopic Properties of Cuprate Superconductors

Michael Norman

Materials Science Division

Argonne National Laboratory

Juan Carlos Campuzano – UIC/ANL

Adam Kaminski – UIC

Stephan Rosenkranz - ANL

Helen Fretwell – Swansea

Joel Mesot – PSI

Hong Ding – Boston

Mohit Randeria – Tata

Matthias Eschrig - ANL

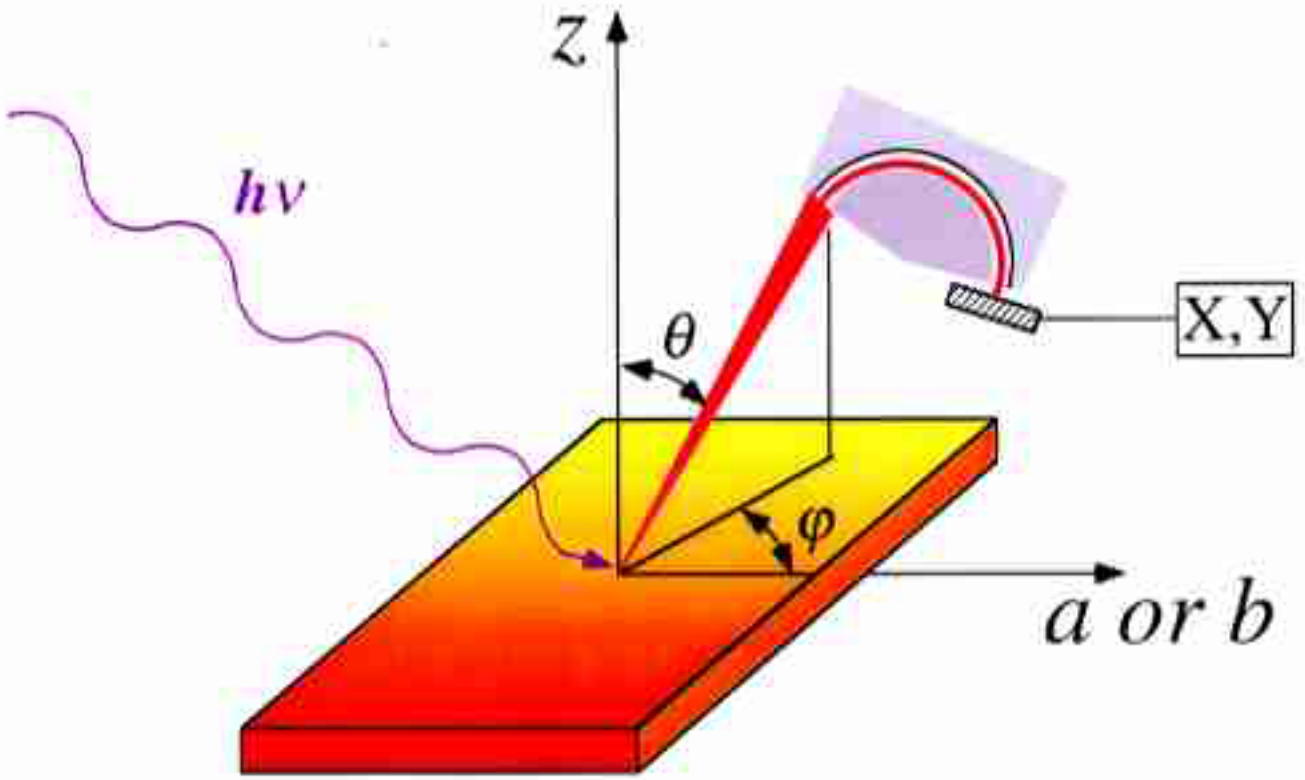

$$k_{//} = \sqrt{\frac{2mE}{h^2}} \sin\theta$$

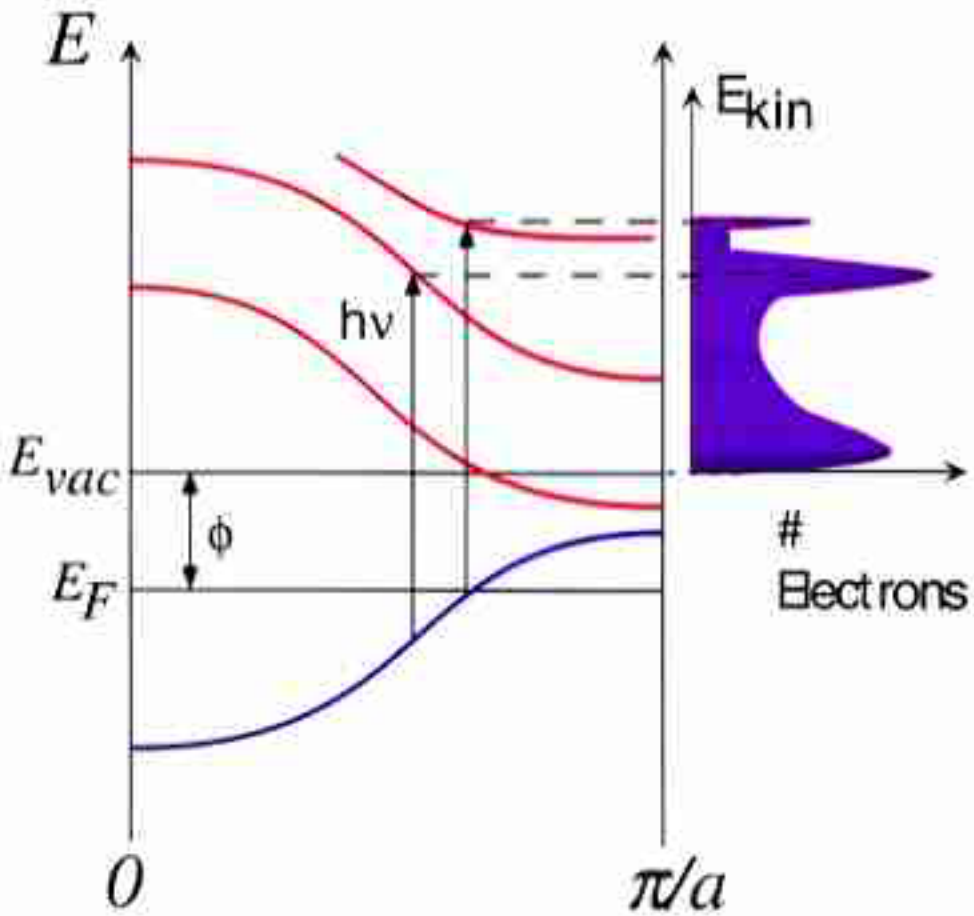

$$I \propto \left| \langle \psi_f \left| \mathbf{A} \cdot \mathbf{p} \right| \psi_i \rangle \right|^2$$

Value of ARPES

IF

1. The sudden approximation is valid
2. The material is quasi two dimensional
3. Modulo dipole matrix elements, resolution, etc.

THEN

One measures the single particle spectral function

$\pi A(\mathbf{k},\omega) = \mathrm{Im}(G)$

where G is the electron Greens function

This allows us to determine

1. Energy dispersion
2. Electron self-energy
3. Superconducting energy gap

$$I(\mathbf{k},\omega) = c_{\mathbf{k}} \int d\mathbf{k}' \int d\omega' \, A(\mathbf{k}',\omega') \, f(\omega') \, R(\omega,\omega')$$

+ "second order light"

+"background"

$$A(\mathbf{k},\omega) = 1/\pi \, Im \, G(\mathbf{k},\omega)$$

$$G^{-1}(\mathbf{k},\omega) = \omega - \varepsilon_{\mathbf{k}} - \Sigma(\mathbf{k},\omega)$$

$$n_{\mathbf{k}} = \int d\omega' \, A(\mathbf{k},\omega') \, f(\omega')$$

$$\Sigma_{BCS}(\mathbf{k},\omega) = \Delta_{\mathbf{k}}^{2}/(\omega+\varepsilon_{-\mathbf{k}})$$

$$\rightarrow A(\vec{k},\omega) = u_{\vec{k}}^2 \, \delta(\omega - E_{\vec{k}}) + v_{\vec{k}}^2 \, \delta(\omega + E_{\vec{k}})$$

where $E_k = \sqrt{\epsilon_k^2 + \Delta_k^2}$

Why Bi-2212?

1. beautiful samples
2. natural cleavage plane

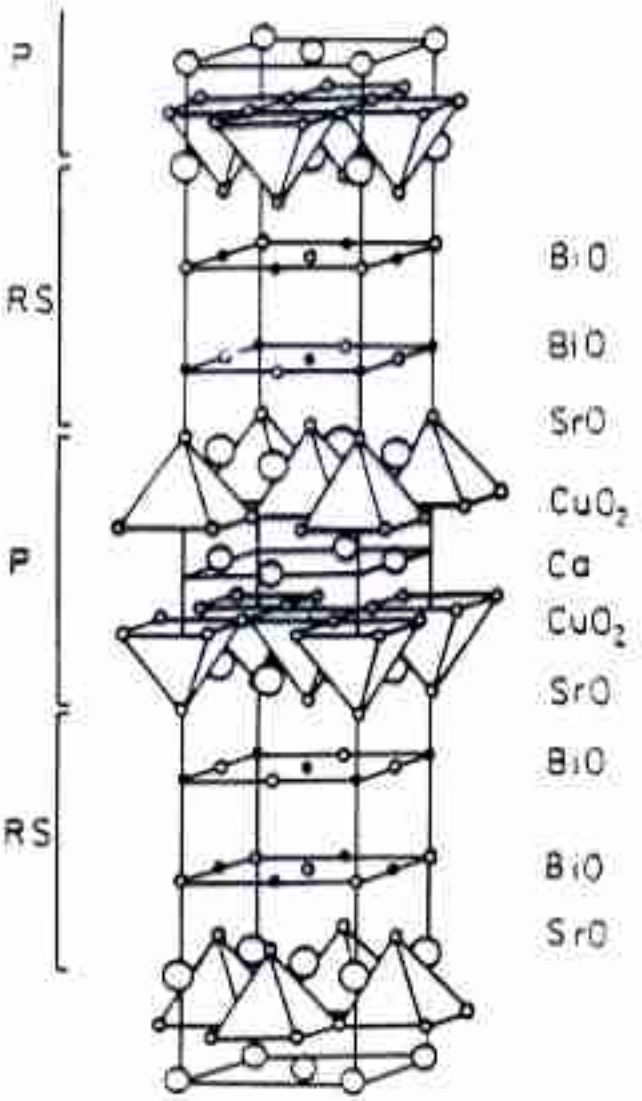

$Q_{FCO} = (\pi, \pi)$

$Q_{SL} = (0.21\ \pi, 0.21\ \pi)$

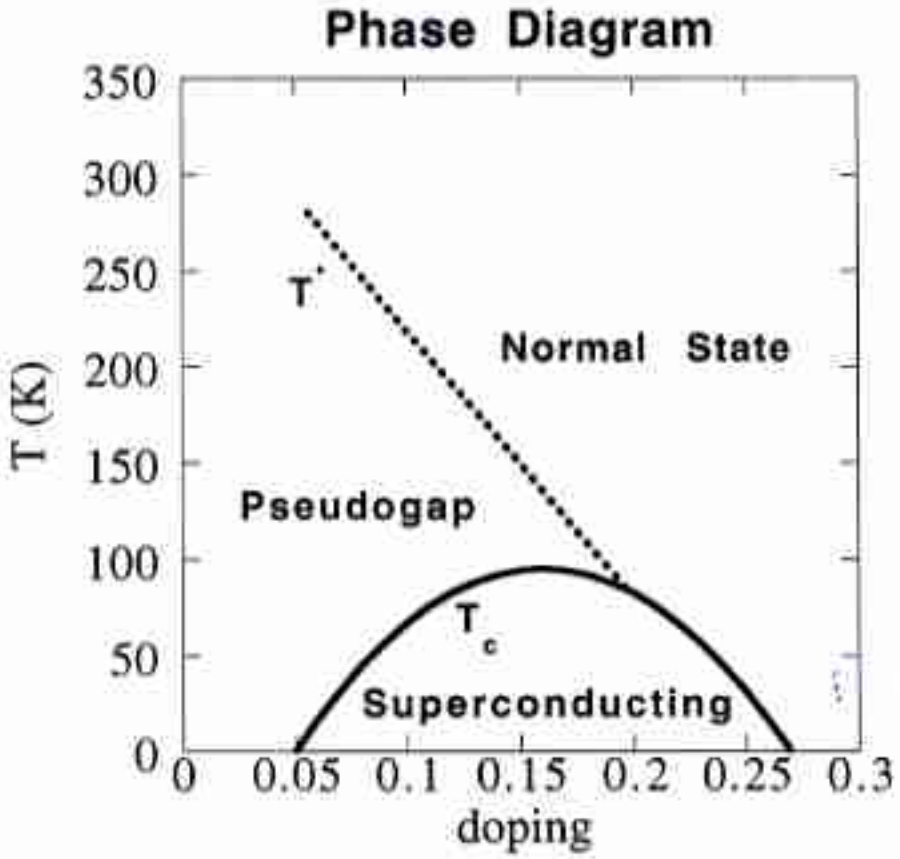
Phase Diagram
350
300
250
200
150
100
50
0
T (K)
T*
Normal State
Pseudogap
T c
Superconducting
0
0.05
0.1
0.15
0.2
0.25
0.3
doping

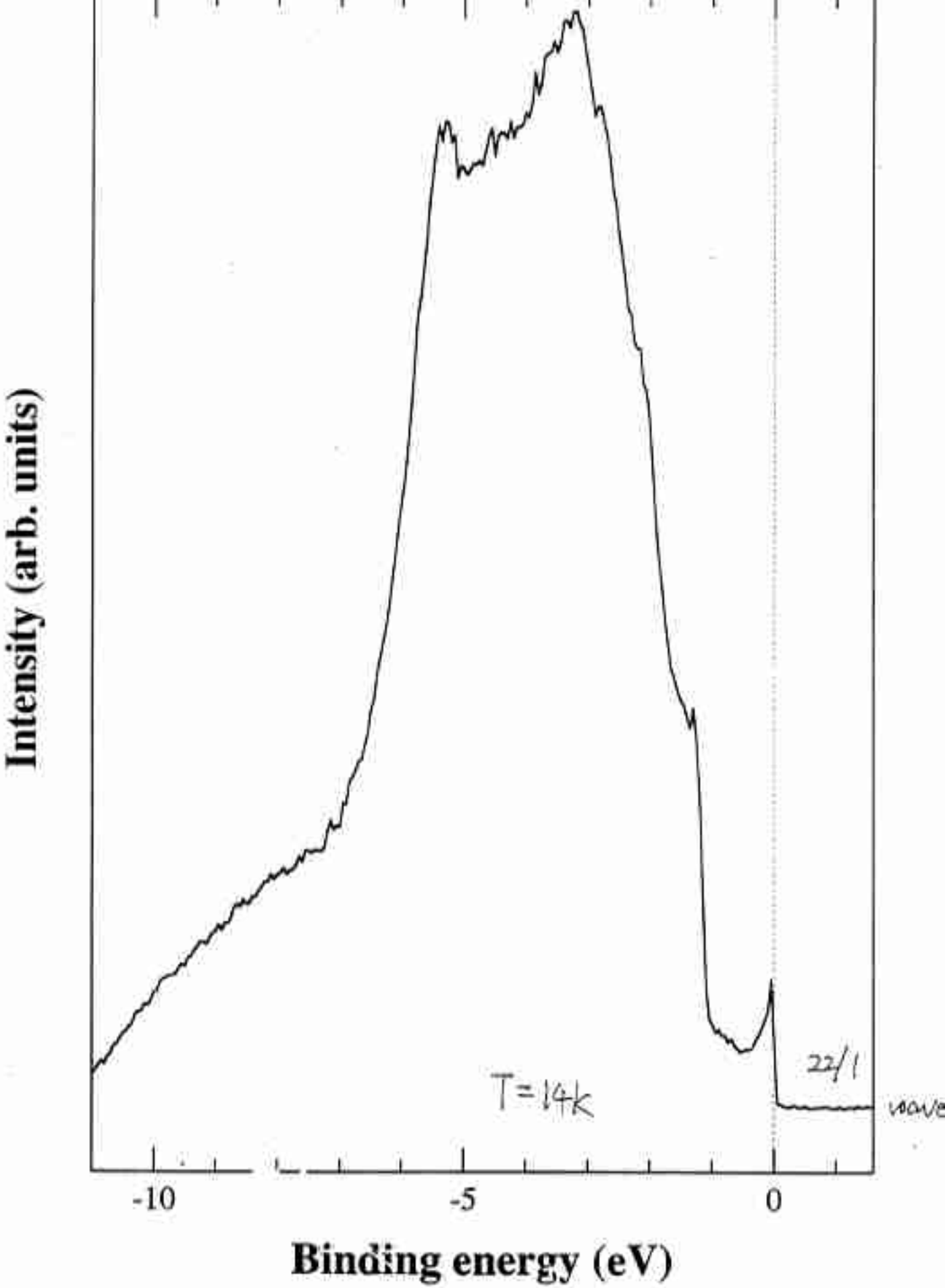
Intensity (arb. units)
T=14K
22/1
-10
-5
0
Binding energy (eV)

0087K

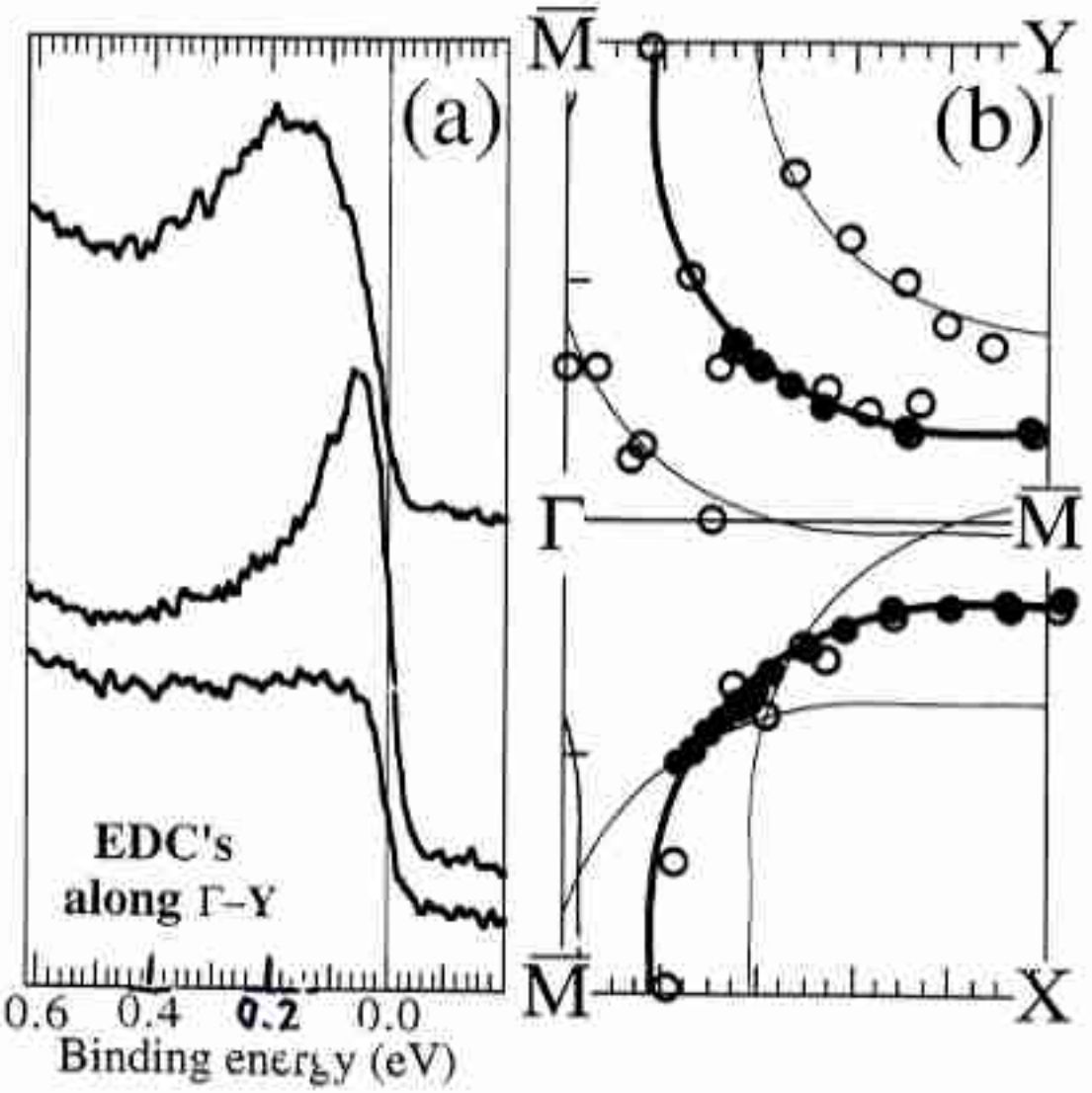

Fig. 1

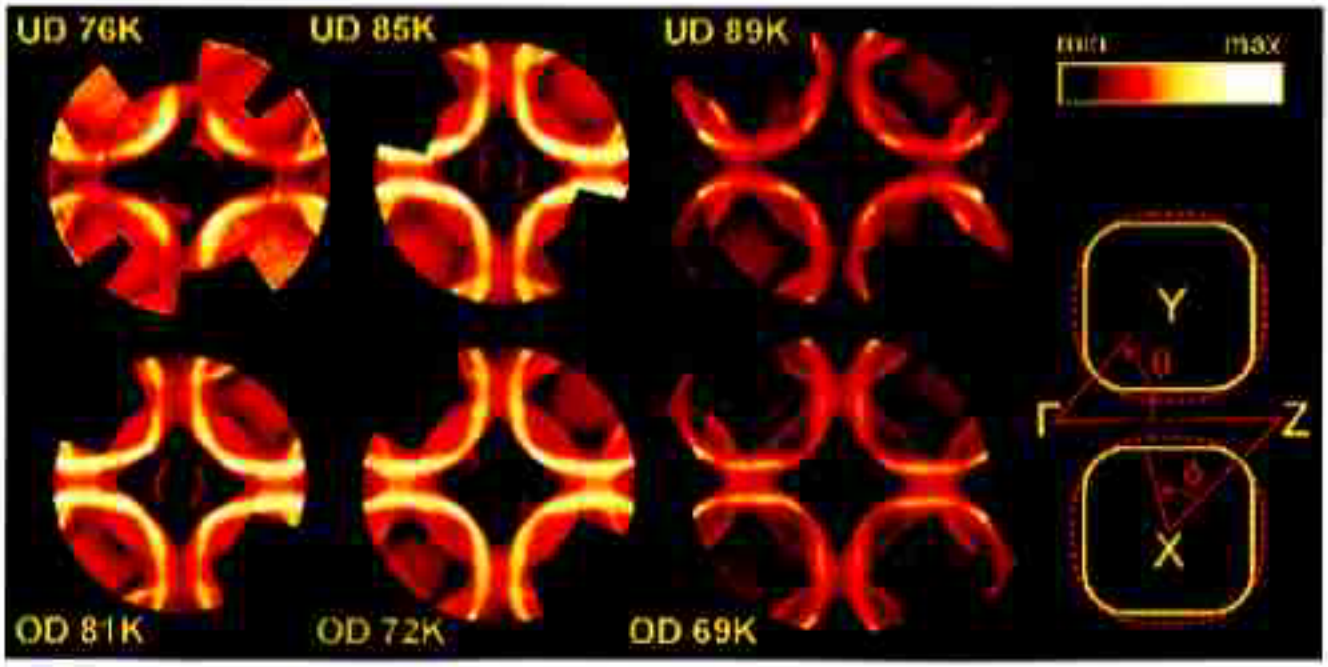

FIG. 1. Basal plane projection of the normal state (300K) Fermi surface of Bi(Pb)-2212 from high resolution ARPES. The E_F intensity (normalized to the signal at $\omega = 0.3$ eV) is shown in color. The T_c of each sample is indicated. The sketch shows the FS for the OD 69K dataset defined by joining the maxima of fits to the normalized E_F MDC's (yellow line).

'barrels' increase in size (as can easily be seen in the decrease of the inter-barrel separation around the M $(\pi,0)$ point), accompanied by an increase in the size of the lenses formed by main FS and shadow FS (SFS). (c) The shape of the FS barrels changes from being quite rounded at low doping to take on the form of a square with well-rounded corners at higher doping. (d) The SFS exists at all doping levels.

We stress that these statements describe experimental observations and are independent of any particular data analysis or physical interpretation.

One of the fundamental questions in the physics of 2D strongly correlated electron systems is to what extent the interacting electron system can be described by models derived perturbatively from the non-interacting case. One way to test this is to consider the validity or otherwise of Luttinger's theorem, which can be paraphrased by stating that the volume (area in 2D) of the FS should be conserved upon switching on the interactions. Thus if we are able to pin down the doping dependence of the exact path in k-space which represents the Fermi surface in, for example, the (Pb,Bi)-2212 HTSC without knowing, a priori, its shape, we would be able to evaluate the doping dependence of the FS area and thus test Luttinger's theorem. The best approach here is to locate the maxima in the E_F momentum distribution curves (MDC's) describing tracks crossing the FS (preferably at right angles) [12,14].

Such a fitting procedure was carried out for the OD 69K sample. The detailed result is well described by a FS having the form of a square with rounded corners, which confirms the visual impression from the intensity map for this sample. A sketch of the fit result is shown as the yellow line on the right hand side of Fig.1. The FS maps from the other samples were then fitted, whereby the extent of the straight sections, as well as the size of the barrel as a whole were varied to optimize the fit to the data. We can then derive the hole concentration x from the simple relation $x = S_h/\Gamma X^2 - 1$, where S_h is the area of main FS barrel.

The results obtained from the analysis of the FS area are shown in Fig.2 in the form of a T_c vs x plot. The solid line shows the commonly employed empirical relation between T_c and x [15]. The surprising result here - for the six samples spanning a total of 35K in T_c - is that the coordinate pairs matching the T_c's to the doping level taken directly from the experimentally determined Fermi surface area also give a parabolic curve (shown as a dotted line), but that this curve is down-shifted in doping by ca. 0.05 towards the underdoped side of the phase diagram.

To explain the discrepancy, the following possibilities spring to mind: (i) the universal T_c vs x curve [15] is not valid for Pb-doped Bi-2212; (ii) the doping level at the surface is not the same as in the bulk; (iii) we are

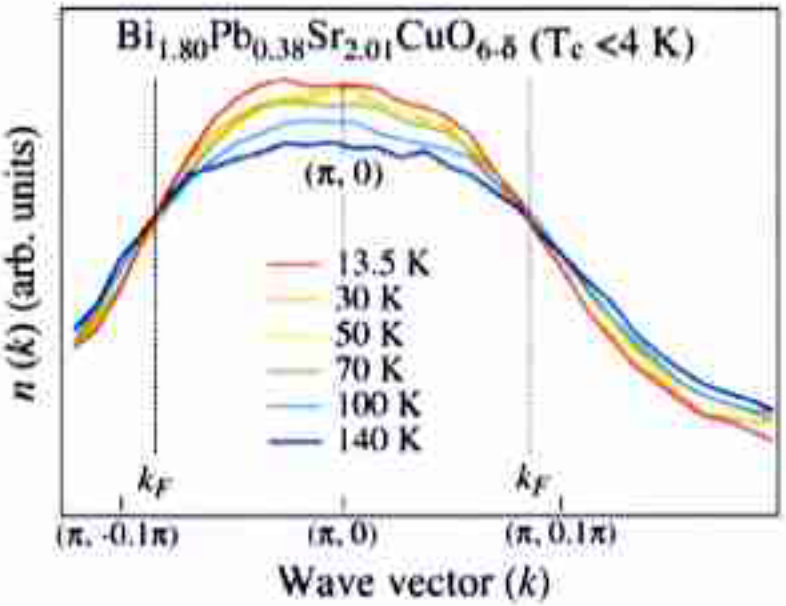

FIG. 3. (Color) Temperature dependence of integrated ARPES intensity $I(k)$ along the $(\pi,0)$-(π,π) cut, obtained by integrating ARPES intensity from 100 to −100 meV binding energy. The angle-integrated-type temperature-independent background is subtracted before integration.

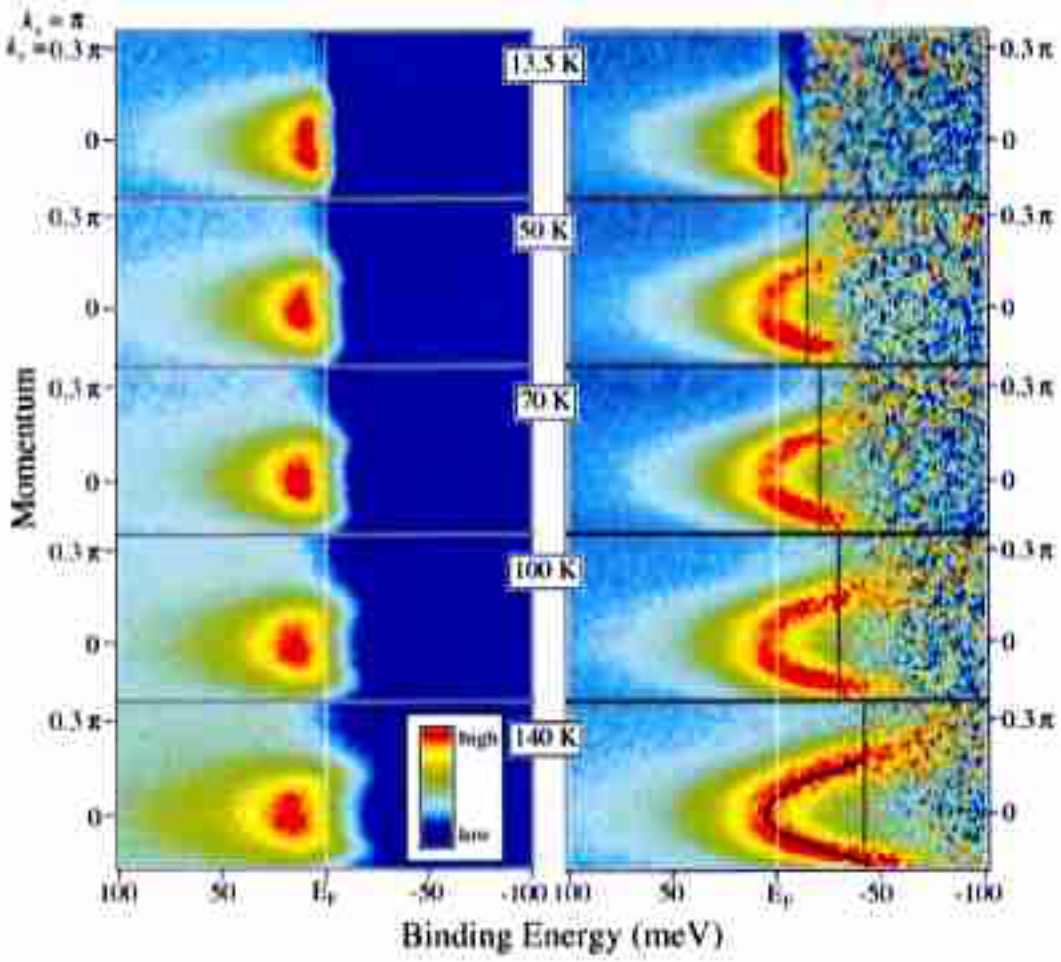

FIG. 4. (Color) Left panel: temperature dependence of ARPES intensity of $Bi_{1.80}Pb_{0.38}Sr_{2.01}CuO_{6+\delta}$ along the $(\pi,0)$-(π,π) cut. Right panel: same divided by the FD function at each temperature convoluted by a Gaussian of a width of energy resolution (11 meV). Dotted lines show the energy above E_F at which the FD function takes a value of 0.03. The solid line in the 140-K data indicates the peak position obtained by fitting with a Lorentzian.

PRB, JUL 95

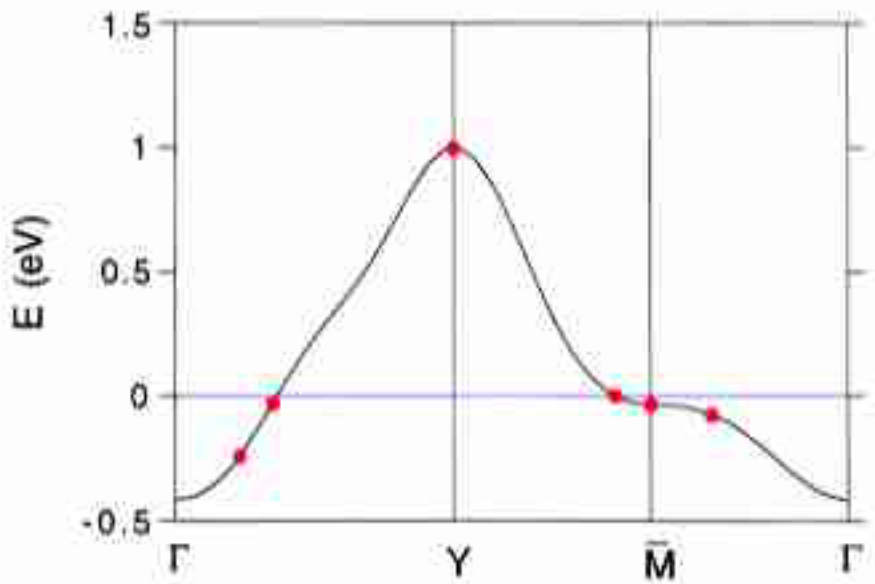

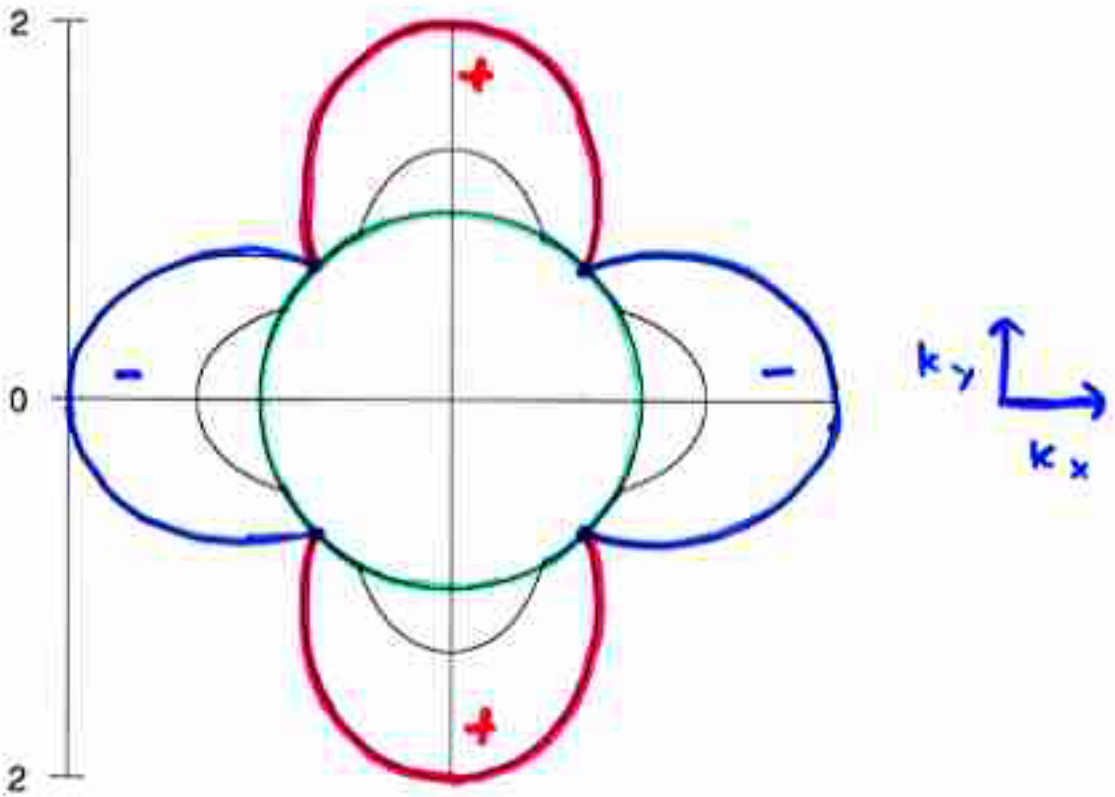

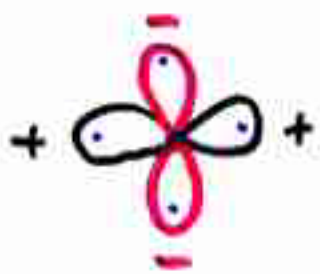

(d-wave SC)

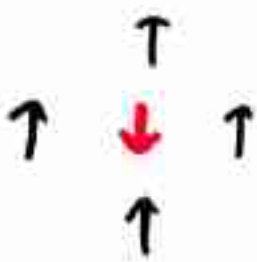

(Neel AF

PRB Oct '96

OD 87K

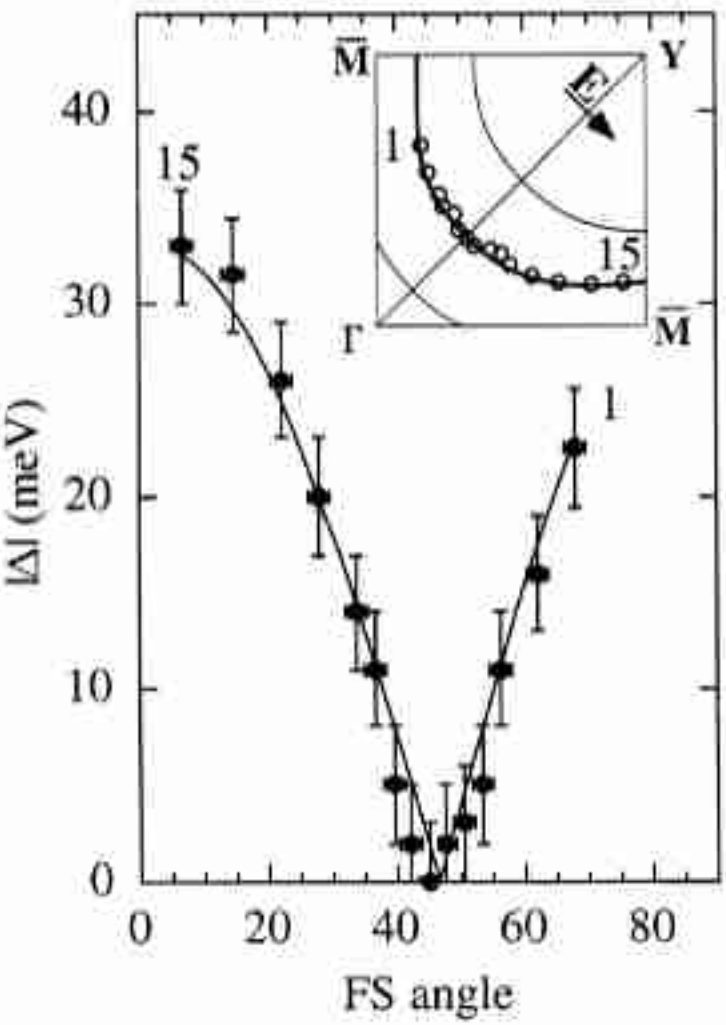

— = $|\cos k_x - \cos k_y|$

Nature Jul '96

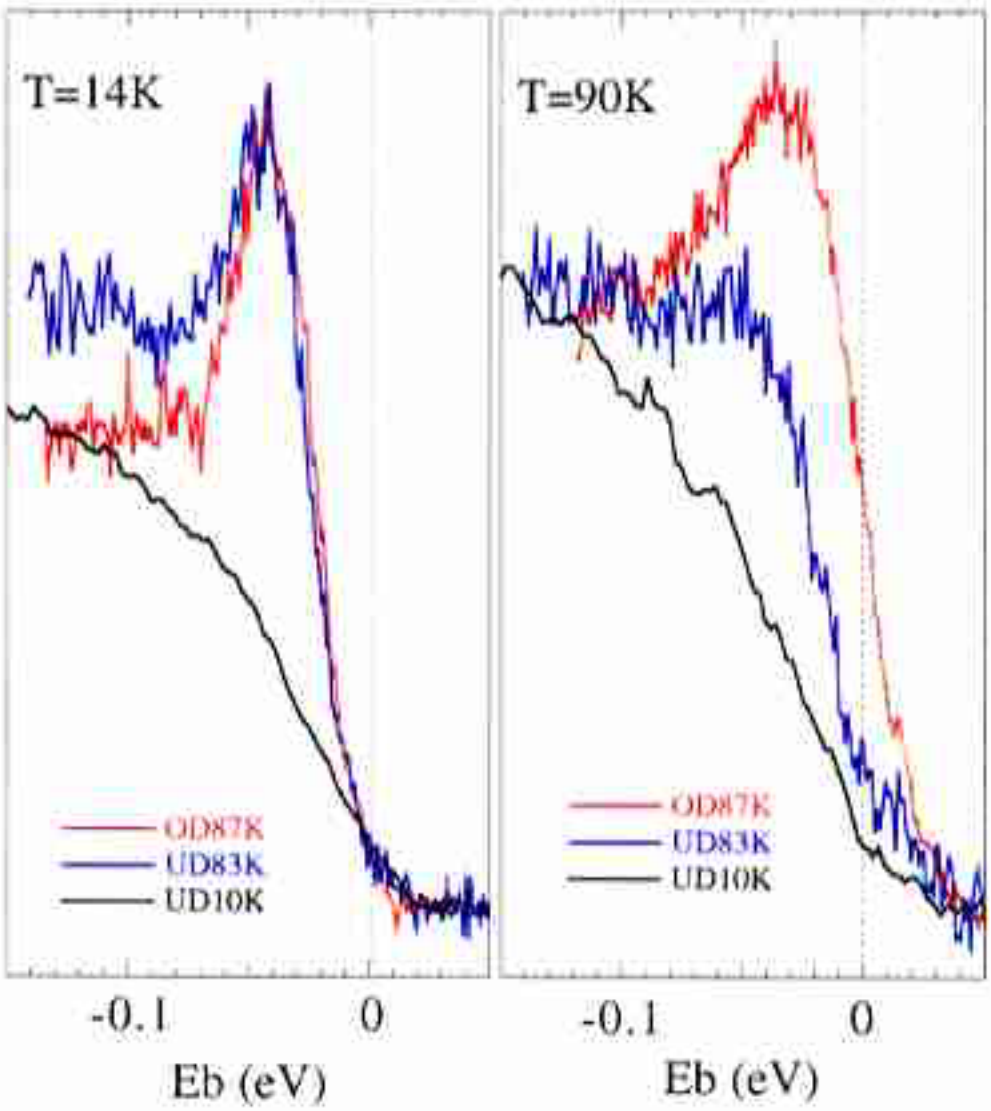

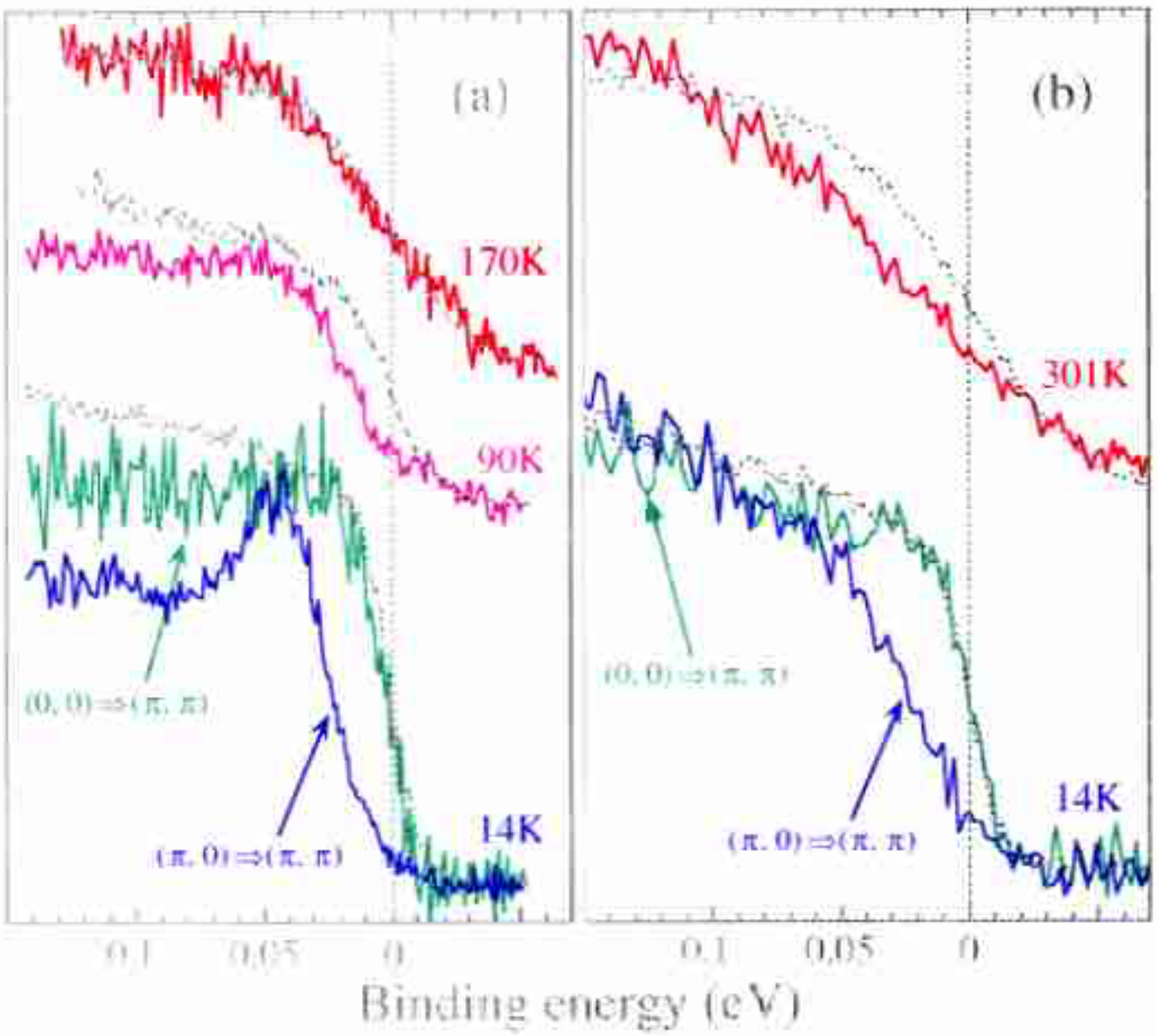
UD 83 K
UD 10 K
(a)
(b)
170K
90K
14K
301K
14K
(0, 0) ⇒ (π, π)
(π, 0) ⇒ (π, π)
(0, 0) ⇒ (π, π)
(π, 0) ⇒ (π, π)
0.1
0.05
0
0.1
0.05
0
Binding energy (eV)

Nature Jul '96

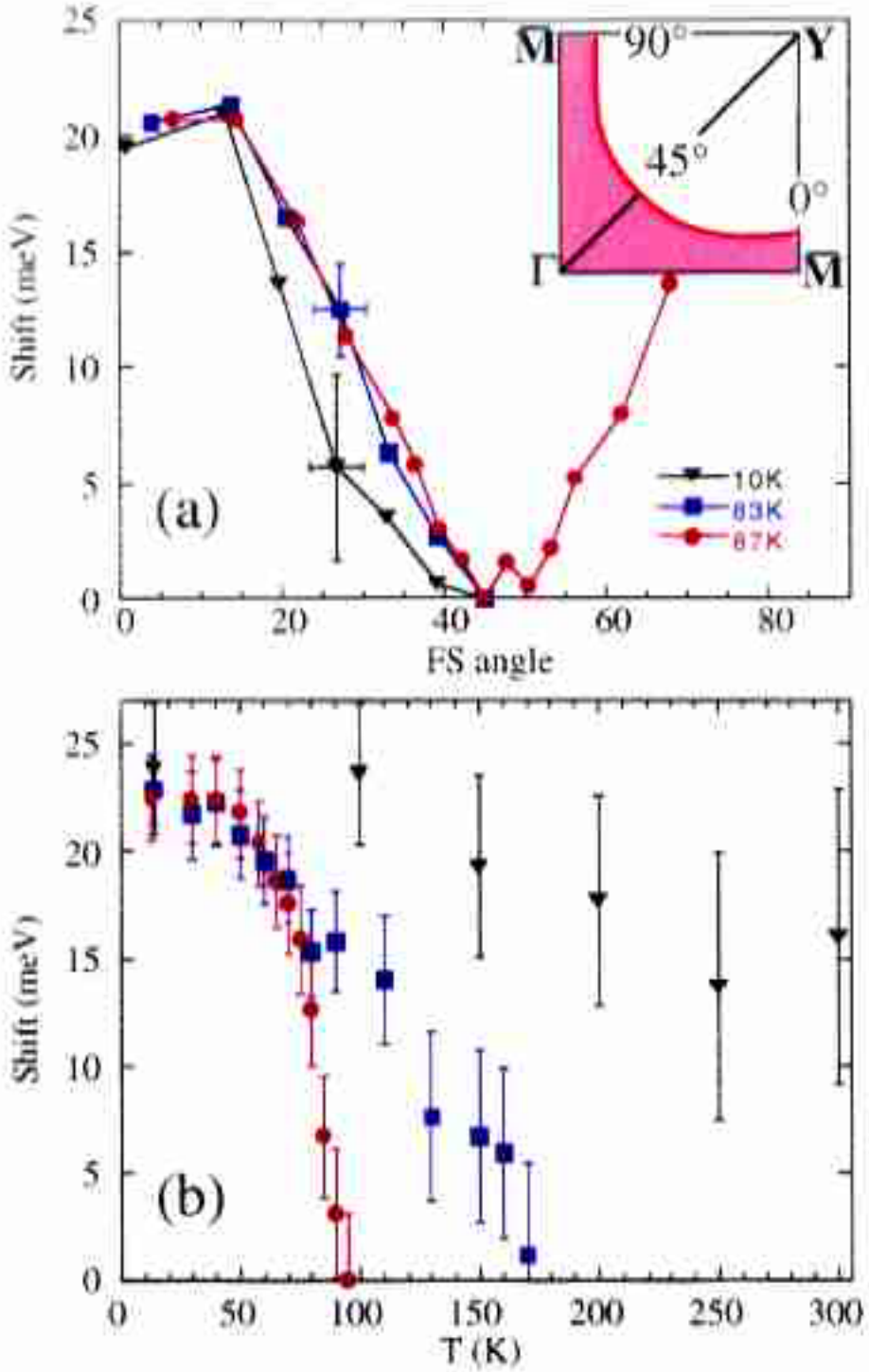

PRL Mar '9

U083K

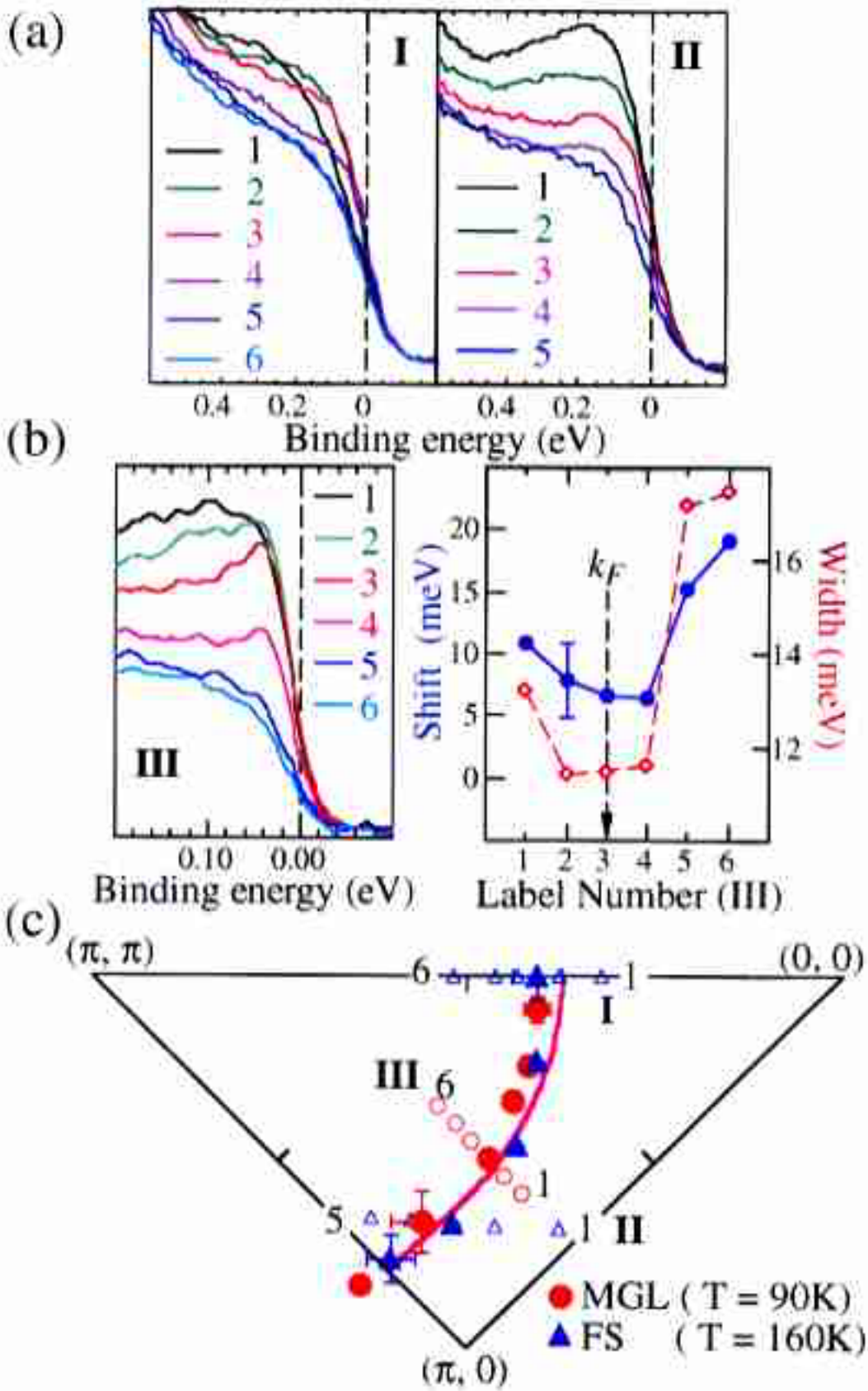

Figure 1 Ding et al.

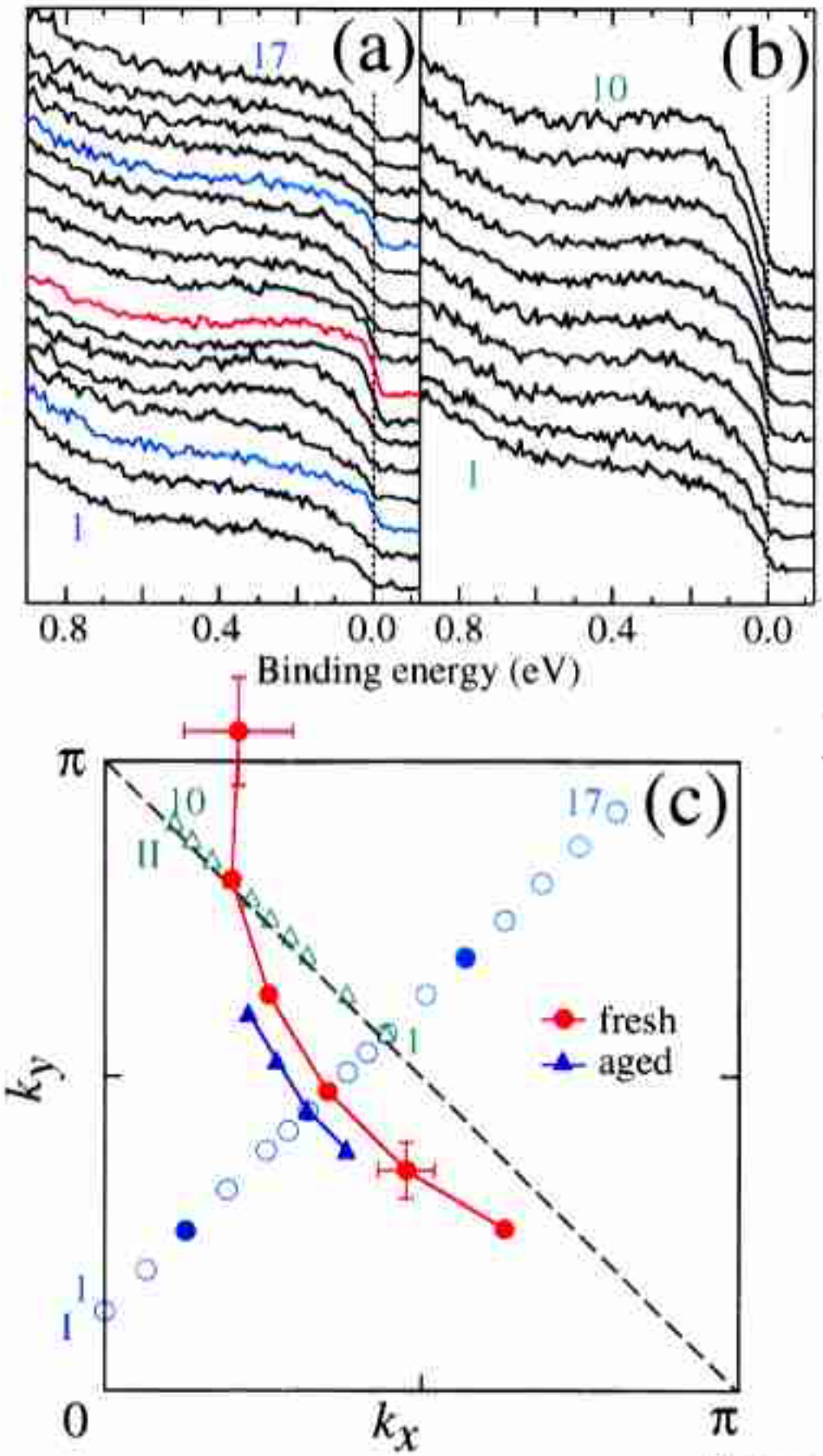

Figure 2 Ding et al

UD 85K

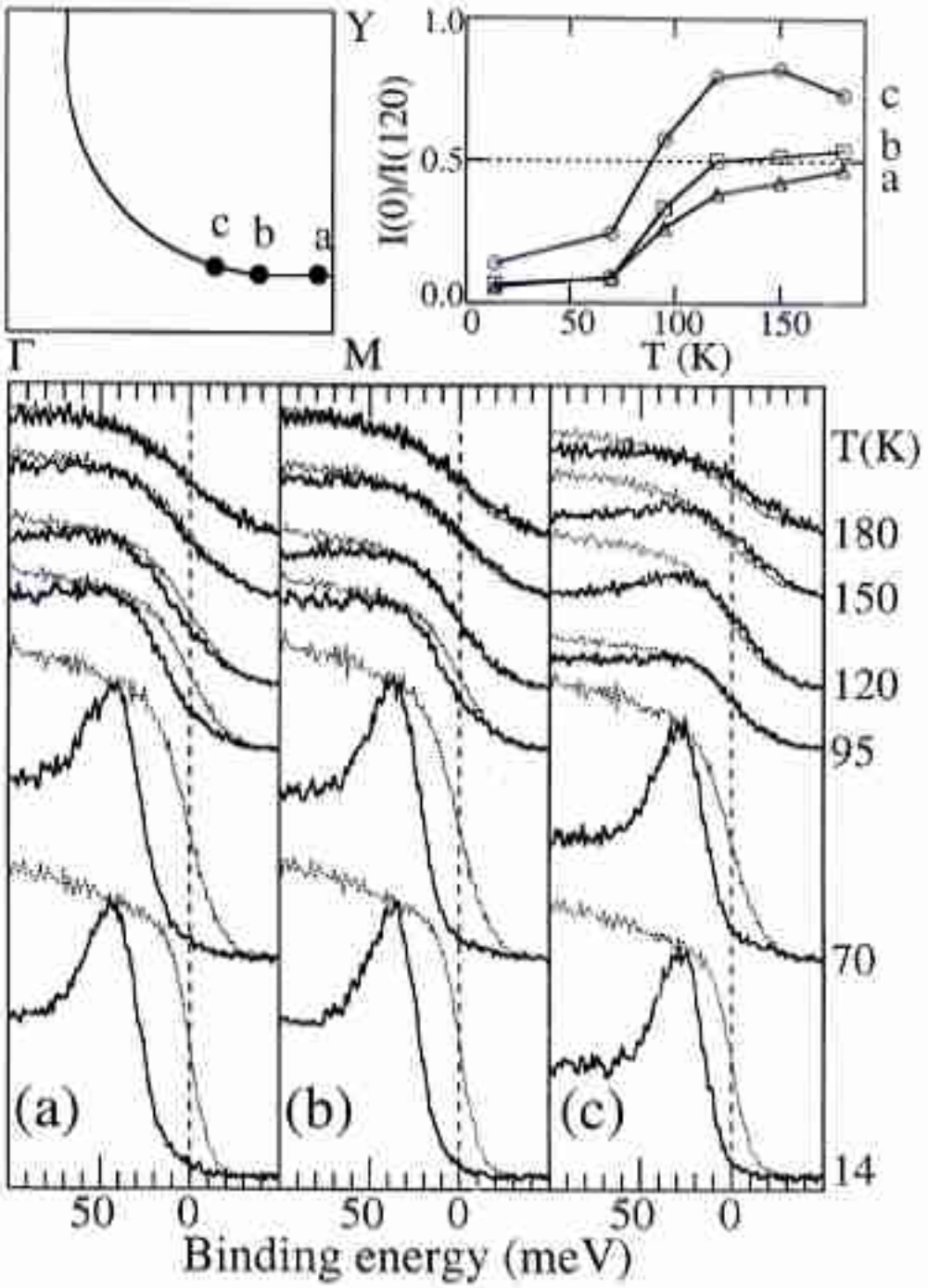

Norman et al. Fig. 2

UD 85K

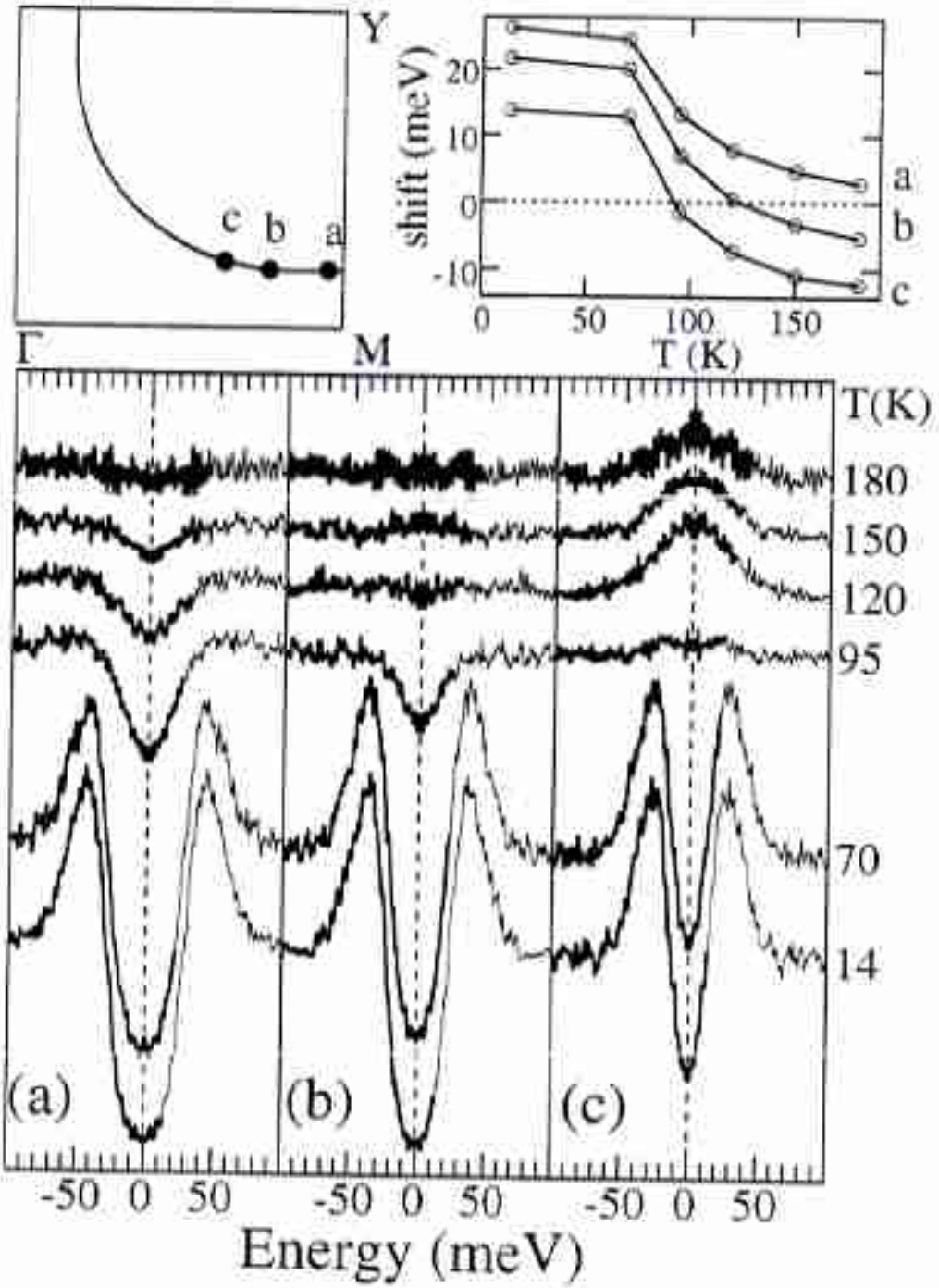

Norman et al. Fig. 4

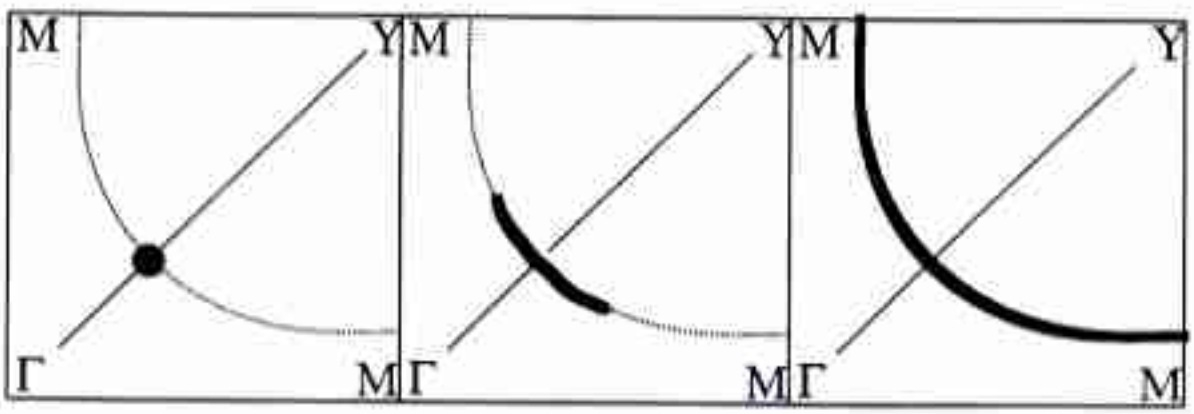

$T < T_c$ $T_c < T < T^*$ $T > T^*$

Norman et al. Fig. 2

Bi2212 UD 83K

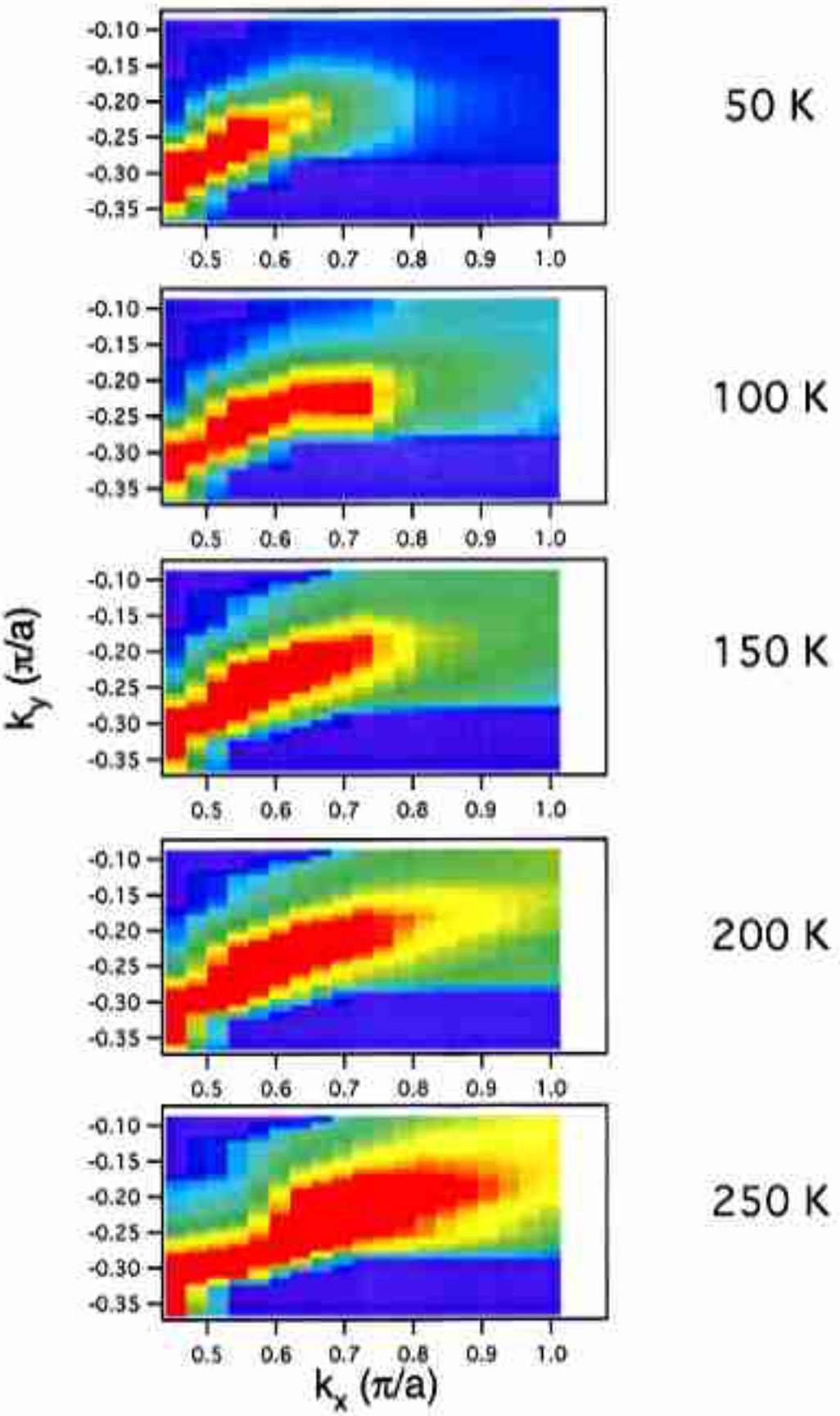

$$\Sigma = -i\Gamma_1 + \Delta^2/(\omega+\varepsilon+i\Gamma_0)$$

Case 1

near $(\pi,0)$ - underdoped

Δ ~ constant with T

$\Gamma_1 \sim T^6$ below T_c

$\Gamma_0 \sim (T-T_c)$ above T_c

Case 2

overdoped; away from $(\pi,0)$ - underdoped

Δ ~ closes at or above T_c

$\Gamma_1 \sim T^6$ below T_c

no Γ_0 (?)

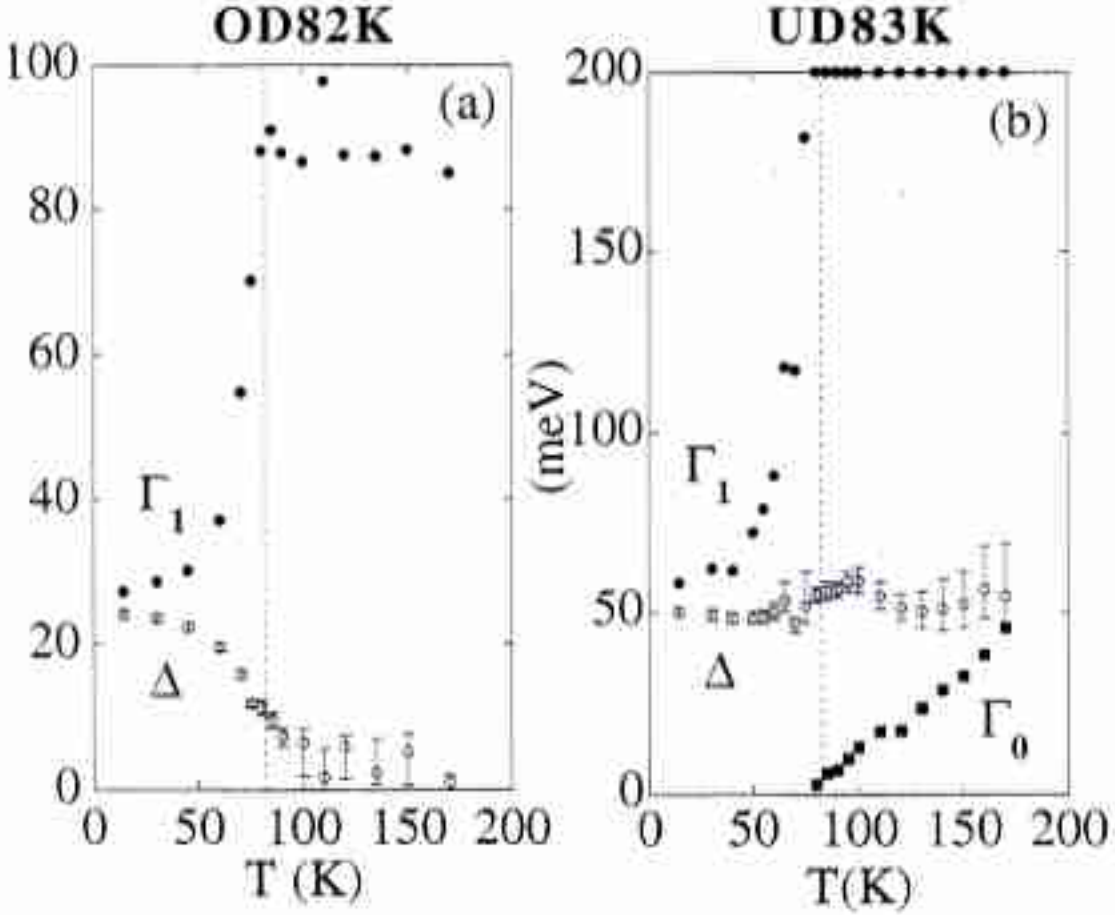
OD82K
(a)
100
80
60
40
20
0
Γ_1
Δ
0
50
100
150
200
T (K)
UD83K
(b)
200
150
100
50
0
(meV)
Γ_1
Δ
Γ_0
0
50
100
150
200
T(K)

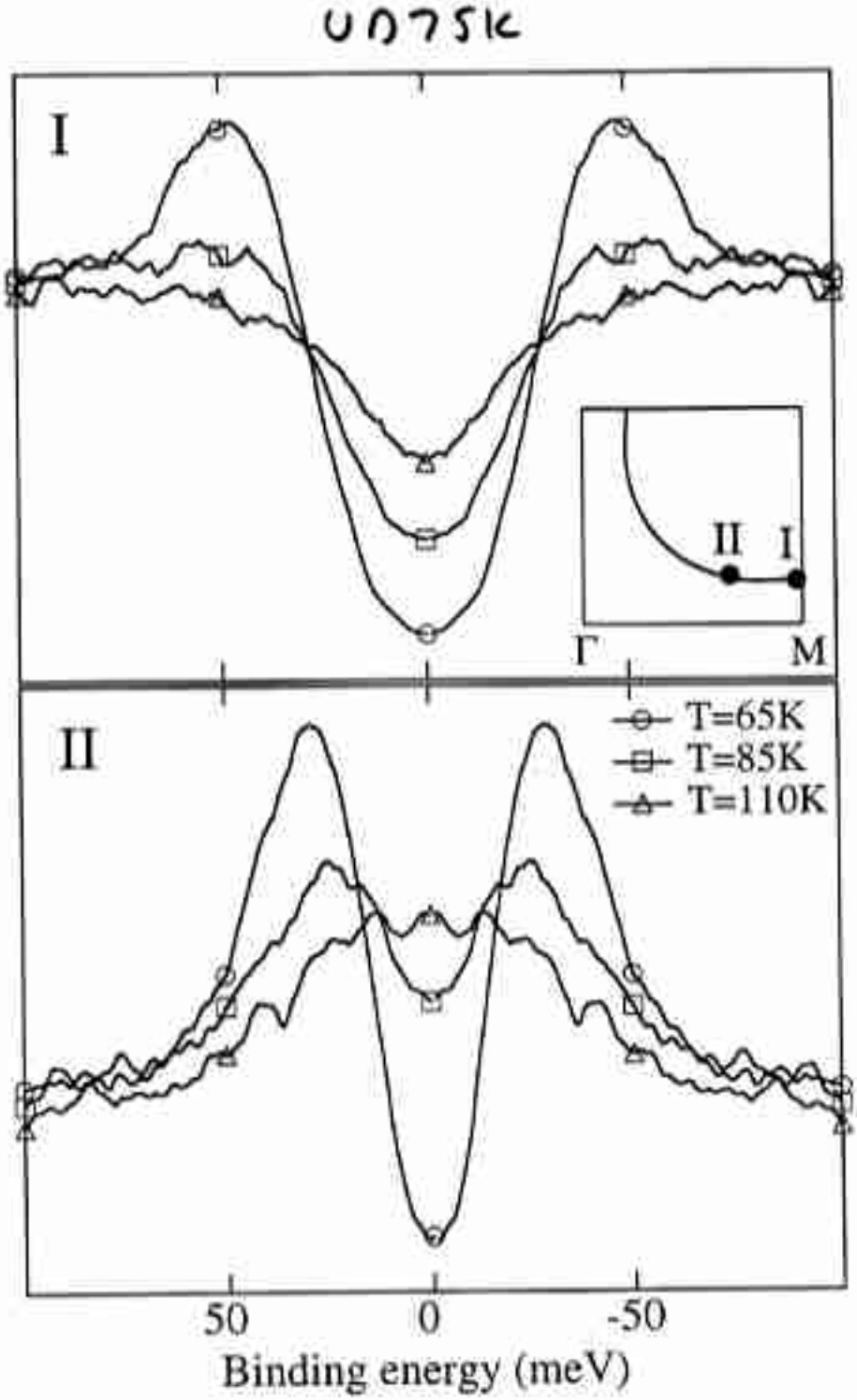

Norman et al. Fig. 5

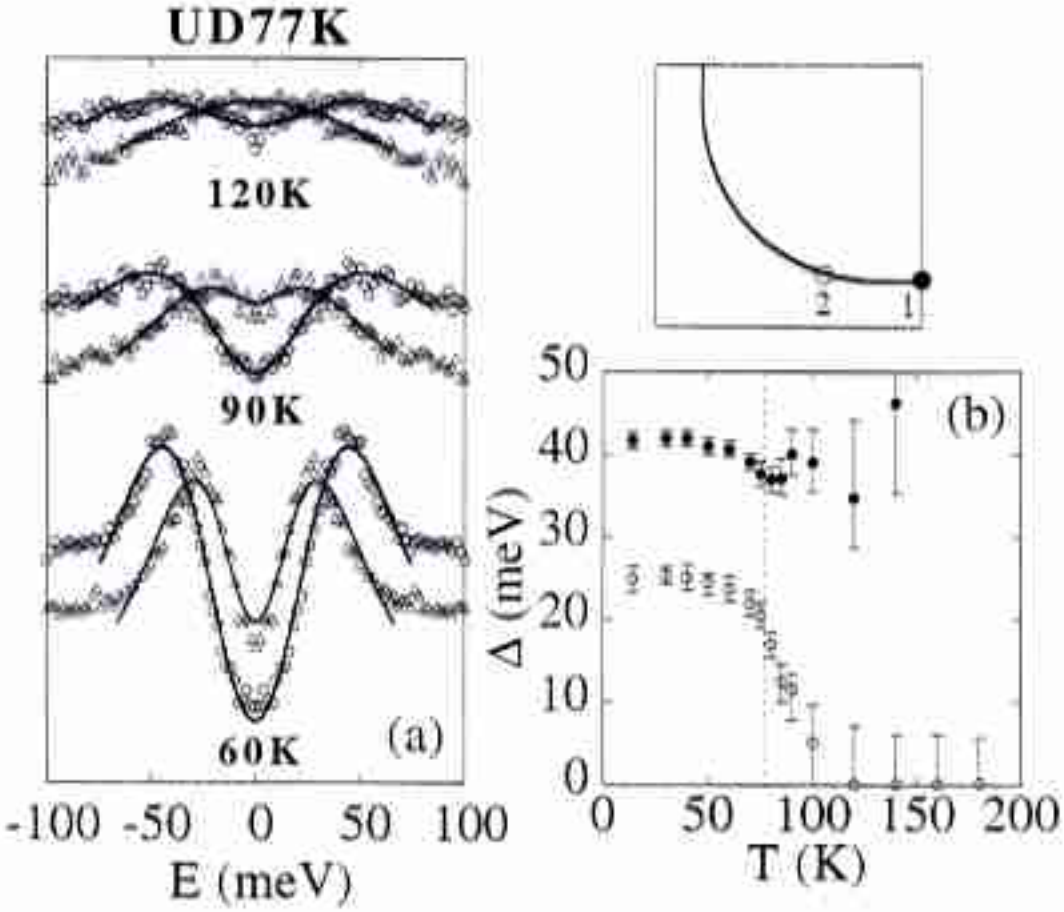
UD77K
120K
90K
60K
(a)
-100 -50 0 50 100
E (meV)
2
1
50
40
30
20
10
0
Δ (meV)
(b)
0 50 100 150 200
T (K)

diagonal to the Cu–O bond direction, but the final state momenta $\mathbf{p}_1$ at point M_1 corresponding to $(\pi,0)$, and $\mathbf{p}_2$ at M_2 corresponding to $(0,\pi)$, are not in this plane. We can see in Fig. 2b and c that the intensity of the spectra at M_1 for the left-circularly polarized (LCP) light is bigger than that for the right-circularly polarized (RCP) light. This situation is exactly opposite at the point M_2 as expected, because this point is a mirror reflection of the point M_1 about m (ref. 14). On the other hand, when the three vectors $\hat{\mathbf{q}}_f$, $\hat{\mathbf{n}}$ and $\mathbf{p}$ are all in a mirror plane m, as illustrated in Fig. 2d where m is the mirror plane along the Cu–O bond direction, there is no dichroism (although the Cu–O bond direction is strictly speaking not a symmetry direction of the crystal in the presence of a superlattice on the Bi–O plane, it was found experimentally[15], and confirmed here, that it is in fact a symmetry direction for the CuO_2 planar electronic states). This is seen in Fig. 2e, where we plot spectra obtained at point M_1 that is now in m. In this case, the spectra have equal intensities to an accuracy of ±0.06%, which sets the overall accuracy of the experiment. As a test, in Fig. 2f we also show spectra from polycrystalline Au, which also do not exhibit dichroism as the orientation of mirror planes is random.

The interesting situation arises when the initial state $|\psi(\mathbf{k})\rangle$ breaks time-reversal symmetry characterized by an order parameter θ. Therefore for $\mathbf{k}$ in some mirror planes m, $|\psi(\mathbf{k})\rangle$ is not an eigenstate of the reflection operator, even though the charge density retains the same lattice symmetries as for $\theta = 0$. In this case, it has been shown quite generally[16] and for a particular case[11] that there is a difference in photoelectron intensity for LCP and RCP light even for $\mathbf{k}$ in m (where the geometrical effect is absent). This effect, proportional to θ, is even for small variations of $\mathbf{k}$ about the mirror plane (while the geometric effect is odd). In order to experimentally detect such a time reversal symmetry breaking (TRSB) state we can plot the energy-integrated intensity[17] (−600 to 100 meV about the chemical potential) of the ARPES signal as a function of the momentum over a very small range (1/20 of the Brillouin zone) along a section perpendicular to the mirror plane. In the absence of TRSB, the energy-integrated intensity as a function of momenta will be a straight line, with the slope changing sign for the opposite circular polarization because of the odd symmetry of the geometrical effect. The two lines will cross at the mirror plane where both LCP and RCP intensities are equal. If upon cooling a TRSB state emerges, it will lead to a difference between the RCP and LCP at the symmetry plane.

In Fig. 3a we show the experimental geometry, and Fig. 3b shows the energy-integrated intensity I_L and I_R as a function of momentum along a section indicated in Fig. 3a for an overdoped ($T_c = 64$ K) sample which does not exhibit a pseudogap[1,2], as seen from the energy spectra at $\mathbf{k}_f$ in Fig. 3d. In Fig. 3c we plot the dichroism signal $D = (I_R - I_L)/(I_R + I_L)$ obtained from the data shown in Fig. 3b. We see that the dichroism signal is independent of temperature and vanishes at the mirror plane, indicating the absence of TRSB in this sample (The non-zero D away from the mirror plane is just the geometric effect discussed above).

We now perform the same measurements on an underdoped sample with a T_c of 85 K, which has a pseudogap and therefore does exhibit a change of the leading edge position of the photoemission

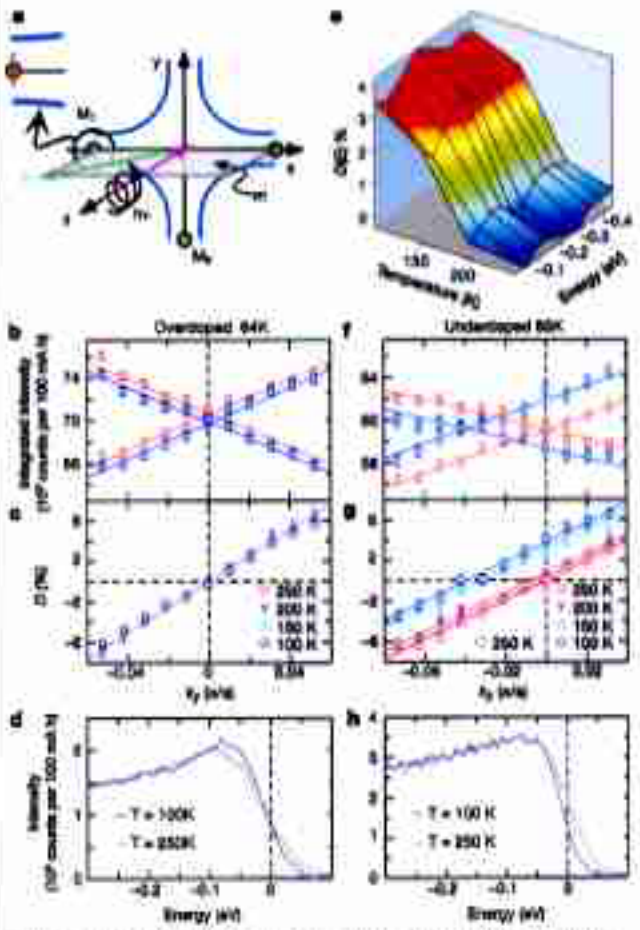

Figure 3 Results of dichroism experiments in overdoped and underdoped samples. **a**, Geometrical arrangement for the experiment, where the incident photon direction, the final state momentum and the normal to the surface are all in the mirror plane. The left side shows an enlarged region around the $(\pi,0)$ point and the range (red line) covered by the detector. **b**, Energy integrated intensity as a function of momentum perpendicular to the mirror plane at the M_1 point of the BZ for LCP and RCP for an overdoped ($T_c = 64$ K) sample for $T = 250$ K (red) and $T = 100$ K (blue). The lines are linear fits to the data. The data were normalized to the second order. The error bars are statistical only and represent one standard deviation. **c**, Relative difference $D = (I_L - I_R)/(I_L + I_R)$ of the data shown in b and in addition for $T = 200$ K (purple) and 150 K (light blue), indicating no circular dichroism for a sample with no shift in the leading edge with temperature. **d**, **e**, Difference signal as a function of temperature and energy, $D(E)$ (integrated over 50 meV). **f**, Energy integrated intensity as a function of momentum perpendicular to the mirror plane at the M_1 point of the Brillouin zone for LCP and RCP for an underdoped sample ($T_c = 85$ K) that displays a shift in the leading edge (h), showing no dichroism for $T = 250$ K but clearly showing that there is dichroism for $T = 100$ K. **g**, Relative difference D of the data shown in f and in addition for $T = 200$ K and $T = 150$ K. The diamond data points for $T = 250$ K were taken at the end of the experiment after a cooling cycle.

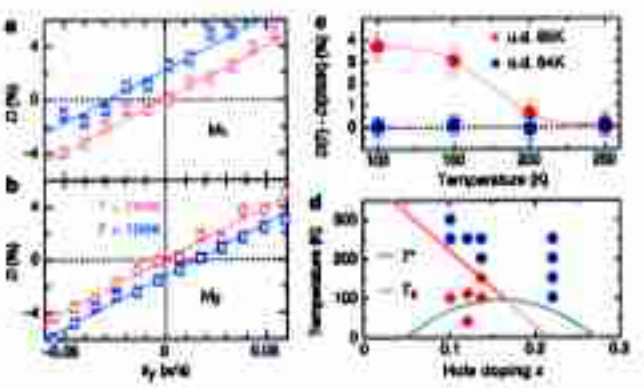

Figure 4 Symmetry and temperature dependence of the observed dichroism. **a**, Relative difference measured for an underdoped sample at M_1 and **b**, after rotating the sample by 90° at M_2. **c**, Temperature dependence of the dichroism signal at M_1 from the data shown in Fig. 3c (overdoped, o.d., 64 K) and 3f (underdoped, u.d., 85 K). **d**, Phase diagram of Bi-2212 showing the presence (red diamonds) and absence (dark blue dots) of dichroism at the mirror plane along the Cu–O bonds.

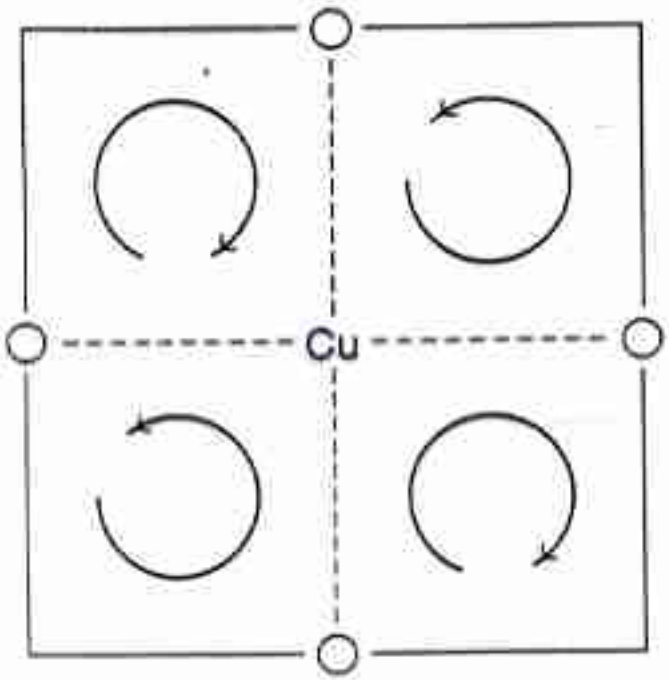

Fig. 6

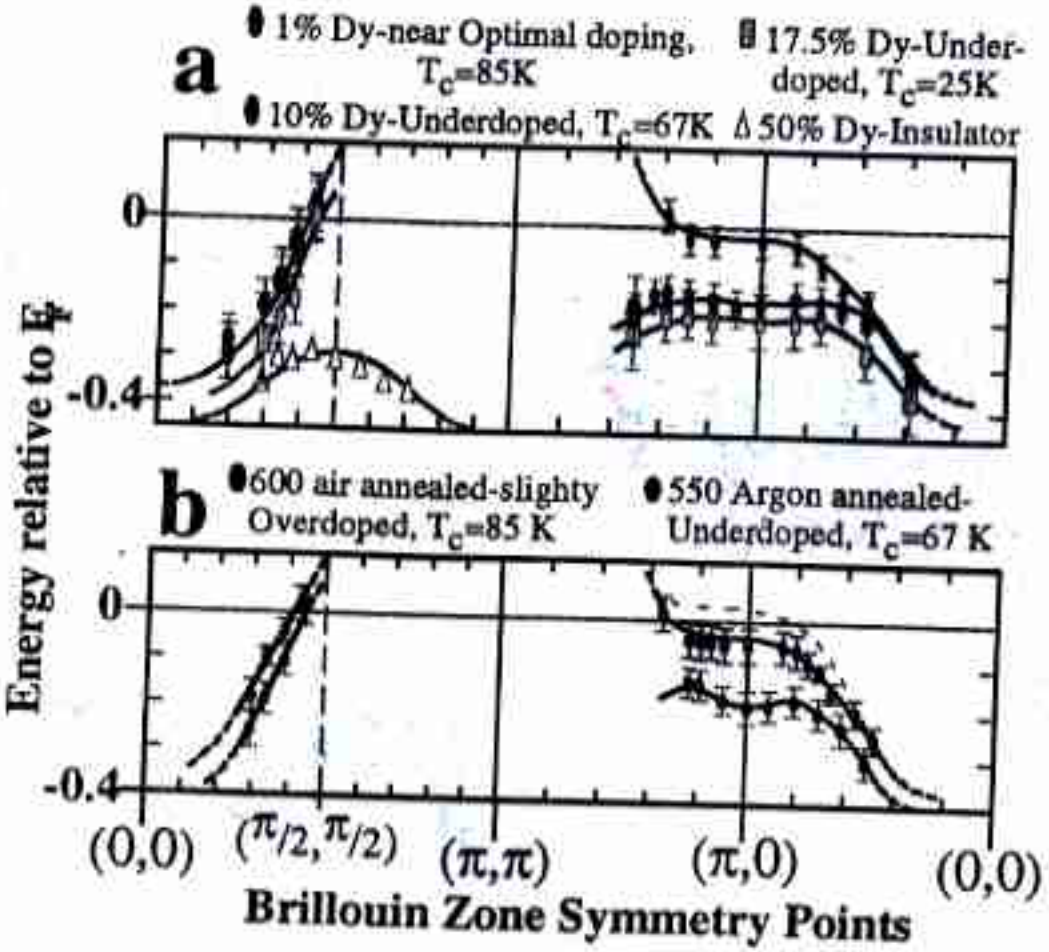
a
1% Dy-near Optimal doping, T_c=85K
17.5% Dy-Under-doped, T_c=25K
10% Dy-Underdoped, T_c=67K
50% Dy-Insulator
0
-0.4
b
600 air annealed-slighty Overdoped, T_c=85 K
550 Argon annealed-Underdoped, T_c=67 K
0
-0.4
Energy relative to E_F
(0,0)
$(\pi/2,\pi/2)$
(π,π)
$(\pi,0)$
(0,0)
Brillouin Zone Symmetry Points

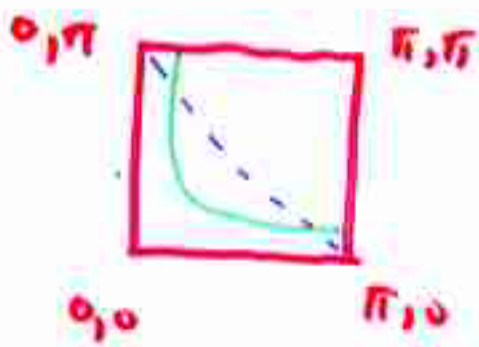
0,π
π,π
0,0
π,0

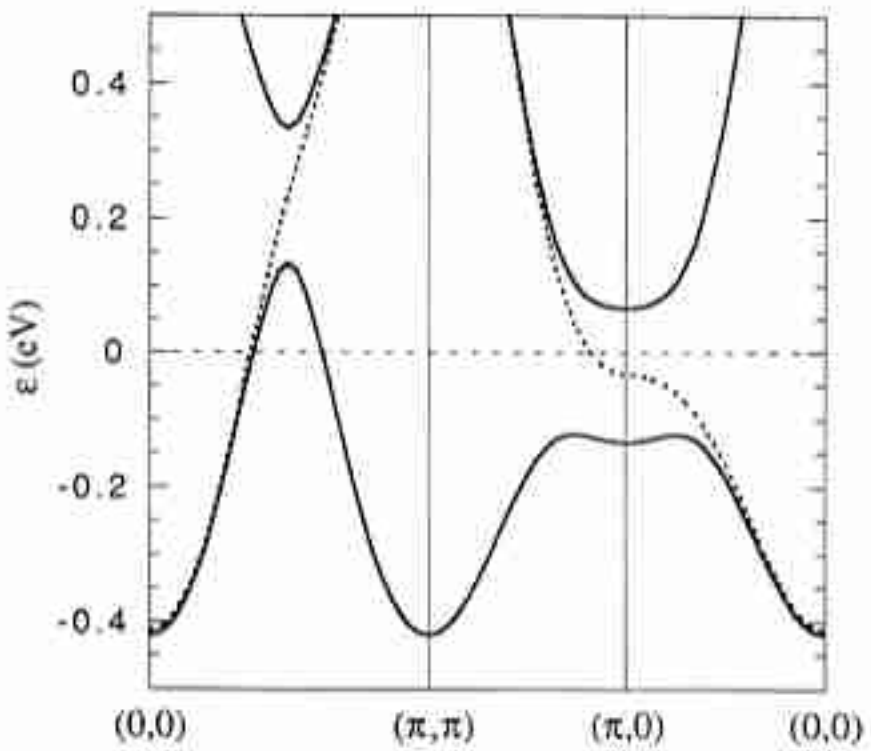
0.4
0.2
0
-0.2
-0.4
ε (eV)
(0,0)
(π,π)
(π,0)
(0,0)

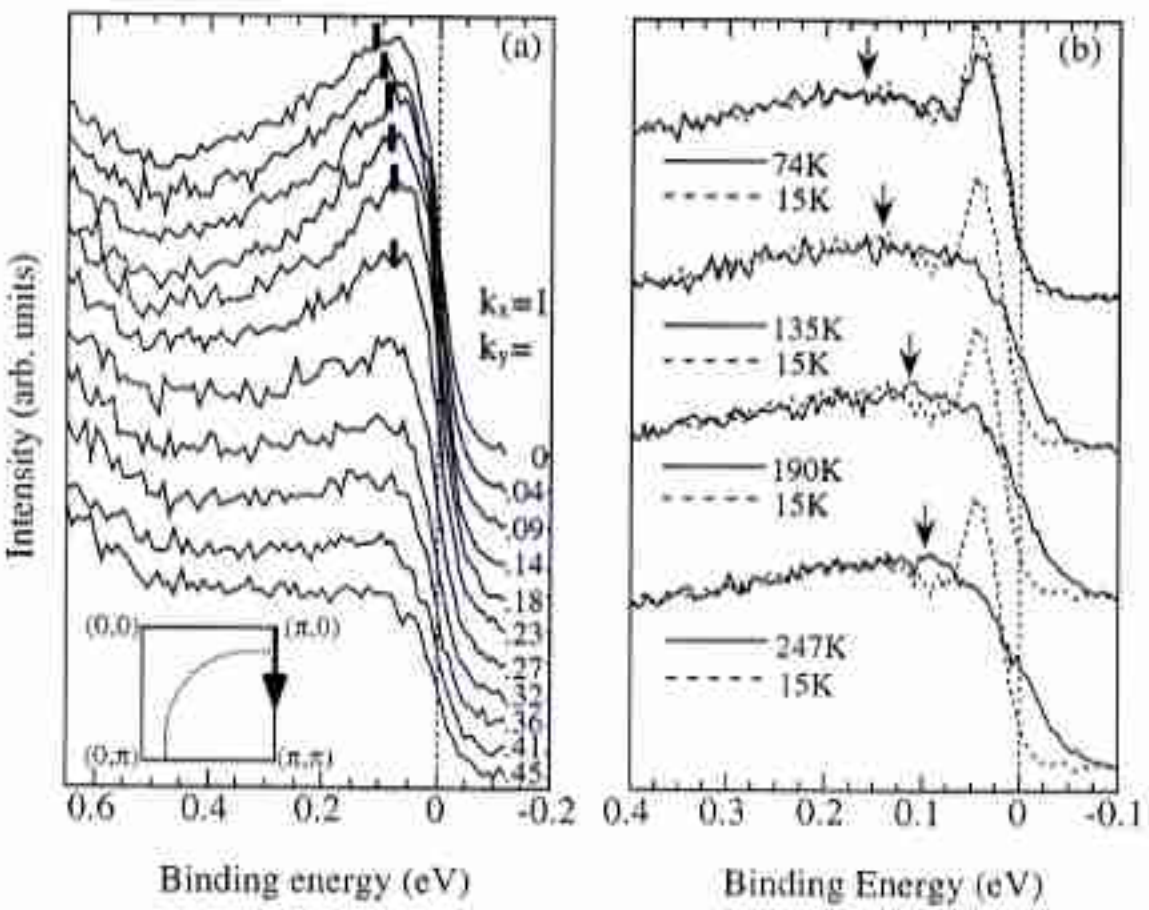

Campuzano, et al. Fig. 1

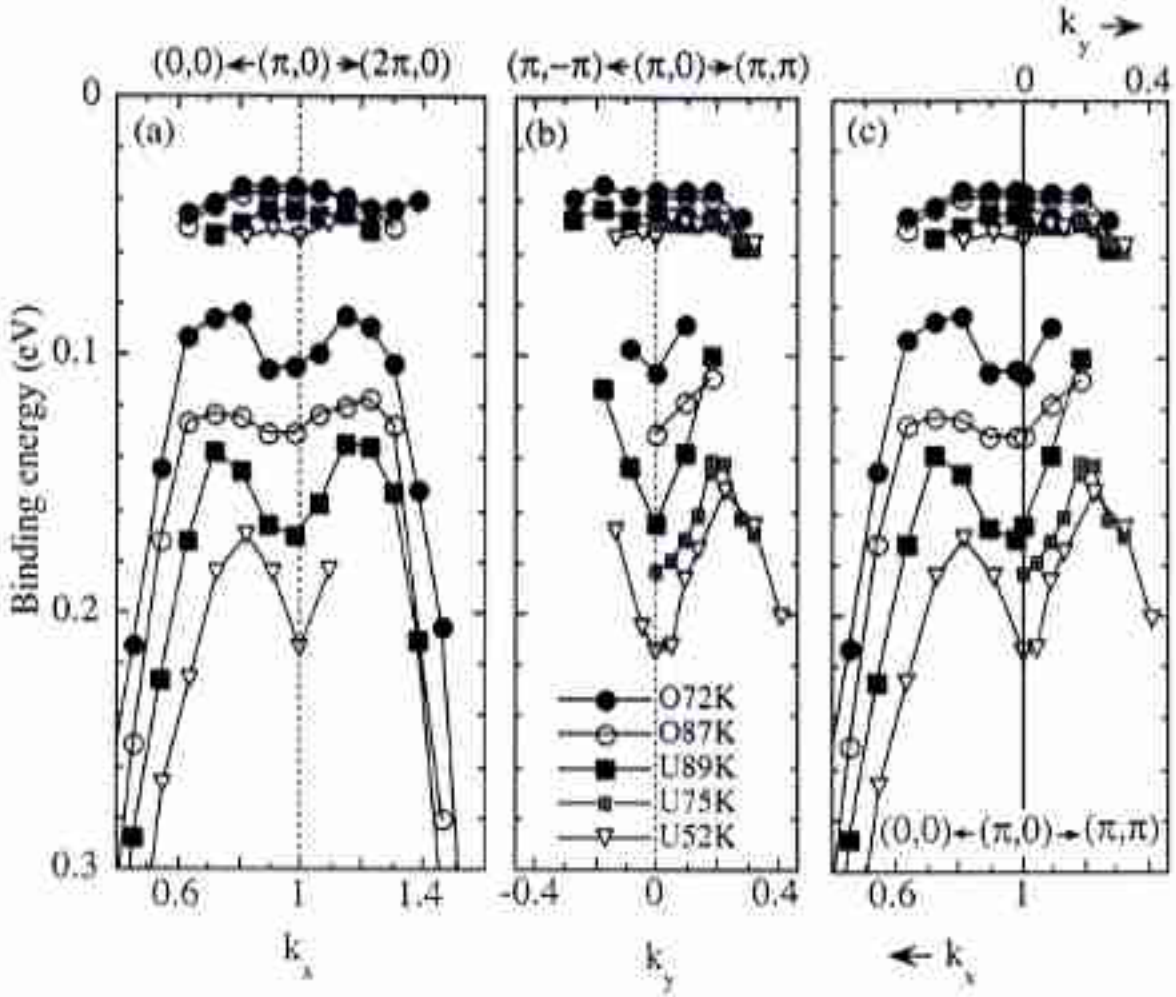

Campuzano, et al. Fig. 3

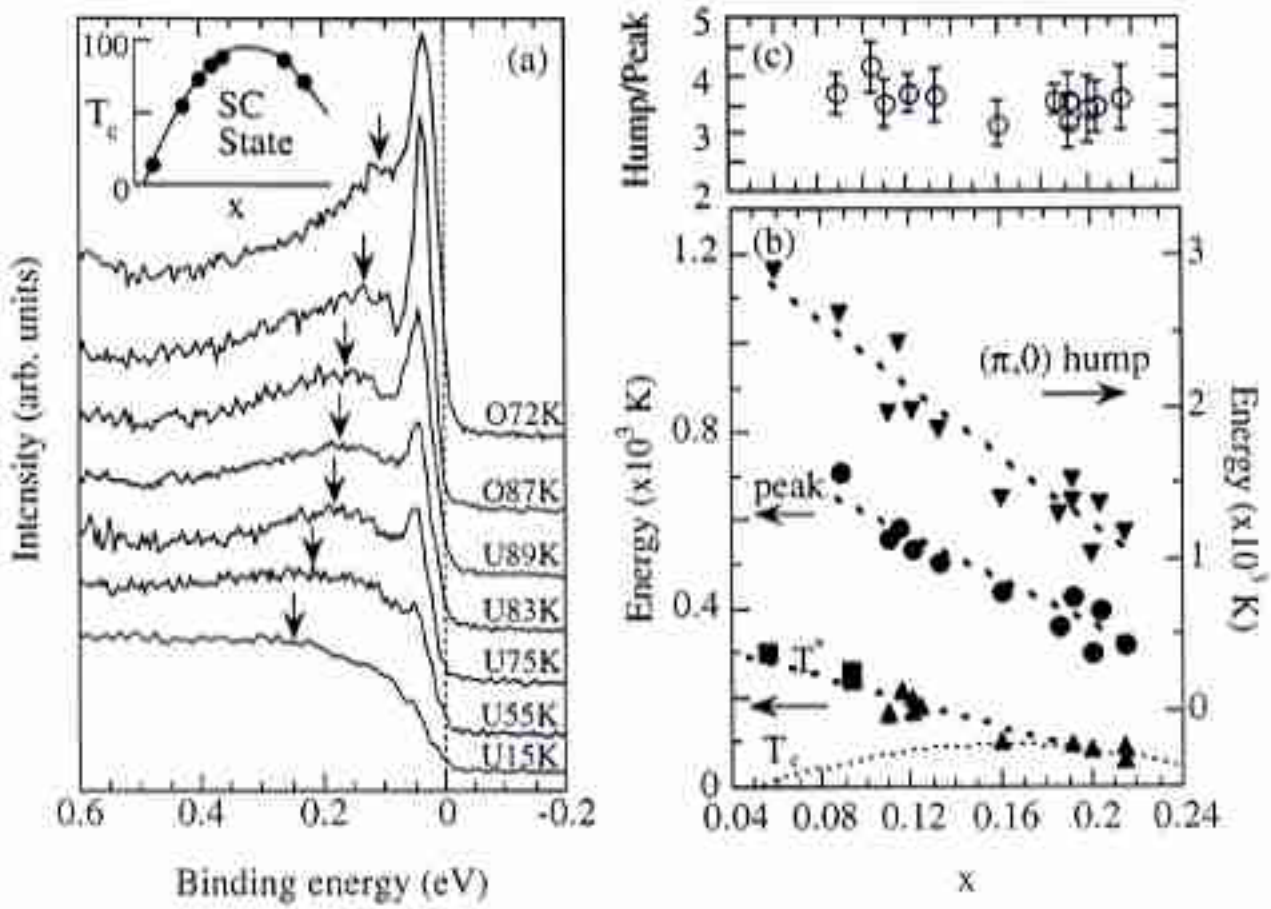

Campuzano, et al. Fig. 4